NASA DEVELOP National Program

University of Georgia
Fall 2016

Eastern India Ecological Forecasting

A Multi-Sensor Approach to Enhance the Prediction of Mangrove Biophysical Characteristics in Bhitarkanika Wildlife Sanctuary and Chilika Lagoon, Odisha, India

DEVELOP Technical Report

Final Draft – November 17, 2016

Abhishek Kumar (Project Lead)
Roger Bledsoe
Caren Remillard
María José Rivera
Jessica Staley
Patricia Stupp

Dr. Deepak Mishra, Department of Geography, University of Georgia (Science Advisor)

1. Abstract

Mangroves, one of the most productive ecosystems on Earth, play a major role in coastal ecosystem processes from mitigating erosion to acting as a barrier against tidal and storm surges associated with tropical cyclones. India has about 5% of the world's mangrove vegetation, and over half of it is found along the east coast of the country. Chilika Lagoon and Bhitarkanika Wildlife Sanctuary are Ramsar sites of international wetland importance that are both situated in the state of Odisha along the east coast of India. Chilika Lagoon holds three small, but distinct mangrove patches, while Bhitarkanika Wildlife Sanctuary has several large, dense patches of mangroves. There is growing concern for the effective management and conservation of these mangrove forests. This study demonstrated the ability to identify early-stage mangrove degradation using data collected from Terra and the Landsat series. Biophysical characteristics of mangroves were determined through the evaluation of chlorophyll content (CHL), leaf area index (LAI), and gross primary productivity (GPP). Sentinel-2 and ASTER data were used to enhance the spatial resolution. Various vegetation indices were implemented to examine band sensitivity in relation to mangrove leaves. The time series developed in this study revealed a phenological pattern for mangrove biophysical characteristics corresponding to different seasons such as higher concentrations during the wet season and lower during the dry season due to fluctuations in salinity and soil moisture content. The results of this study will be used as an efficient and non-destructive biophysical mapping and monitoring protocol for mangrove forests in restoration decision-making.

Keywords

Remote sensing, biophysical parameters, mangrove degradation, MODIS, ASTER, Landsat 8, Sentinel-2

2. Introduction

Mangrove forests are one of the most productive and biologically complex ecosystems on earth. Clustering along tropical coastlines and intertidal zones, they play a unique and crucial role in coastal ecosystem processes. Unlike many other types of vegetation, mangroves can grow in extreme environmental conditions such as high salinity, high temperature, extreme tides, high sedimentation, and anaerobic soils (Giri *et al.*, 2010). This is mainly attributed to their complex root system, which not only allows them to live in such harsh environmental settings, but also helps protect coastlines from storm surges and erosion (Kauffman and Donato, 2012). In addition, mangroves provide many other valuable ecological services including acting as an effective carbon sequester and providing habitat and nurseries for many species of animals (Azam, 2011).

Mangroves are especially important for countries, like India, that frequently face tropical cyclones and monsoons that ravage coastal areas. India has approximately 4,461 km^2 of mangrove habitat, 57% of which are located along the east coast of the country (Pattanaik *et al.*, 2008). Chilika Lagoon and Bhitarkanika Wildlife Sanctuary are two notable east coast wetland sites recognized by the Ramsar Convention on Wetlands and are both situated in the state of Odisha. As the world's second largest brackish water lagoon (Peetabas and Panda, 2015), Chilika Lagoon holds three small, distinct mangrove patches near the lagoon opening to the Bay of Bengal. Bhitarkanika Wildlife Sanctuary lies north of Chilika Lagoon on a delta formed by the Brahmani and Baitarani rivers and has several large, dense patches of mangroves (Fig. 1). Bhitarkanika's mangrove forest is recognized as the second largest mangrove ecosystem in India (Chauhan and Ramanathan, 2008).

With 71 species of mangroves and mangrove associates, Chilika Lagoon and Bhitarkanika Wildlife Sanctuary are known for being biodiversity hotspots supporting several populations of crocodiles, lizards, resident and

migratory birds, and several rare and endangered mammals (Behera and Nayak, 2013). Residents from at least 36 nearby villages also receive valuable resources and services from the mangroves, including food, raw materials, medicinal and ornamental products and vacation/leisure sites (Hussain *et al.*, 2010). Despite their ecological, social, and economic importance, mangroves have been over-exploited or converted to various other forms of land use including agriculture, aquaculture, salt ponds, terrestrial forestry, and urban and industrial developments (Reddy *et al.*, 2007). Additionally, threats like encroachment upon forests, unauthorized aquaculture practices, grazing, and effluent discharge create even more pressure on mangrove forests and local biodiversity (DFE, 2008).

In response, the Government of Odisha's Chilika Development Authority (CDA) partnered with University of Georgia's (UGA) NASA DEVELOP team to conduct an ecological forecasting study on Chilika's and Bhitarkanika's mangrove habitats by using various remote sensing tools and data sources. Satellite imagery and data were acquired from NASA's Terra and Landsat satellites between the years 2013 and 2016 to identify patterns of mangrove growth and degradation. Sentinel-2 data from the European Space Agency (ESA) were also used to enhance the spatial and temporal resolutions. Ultimately, the objective of the project was to develop a mangrove biophysical characteristics prediction tool for the Bhitarkanika Wildlife Sanctuary and Chilika Lagoon by using moderate resolution remote sensing reflectance data. This tool will be used to derive long-term spatio-temporal estimations of mangrove physiological status in order to improve mangrove management and restoration efforts by the CDA.

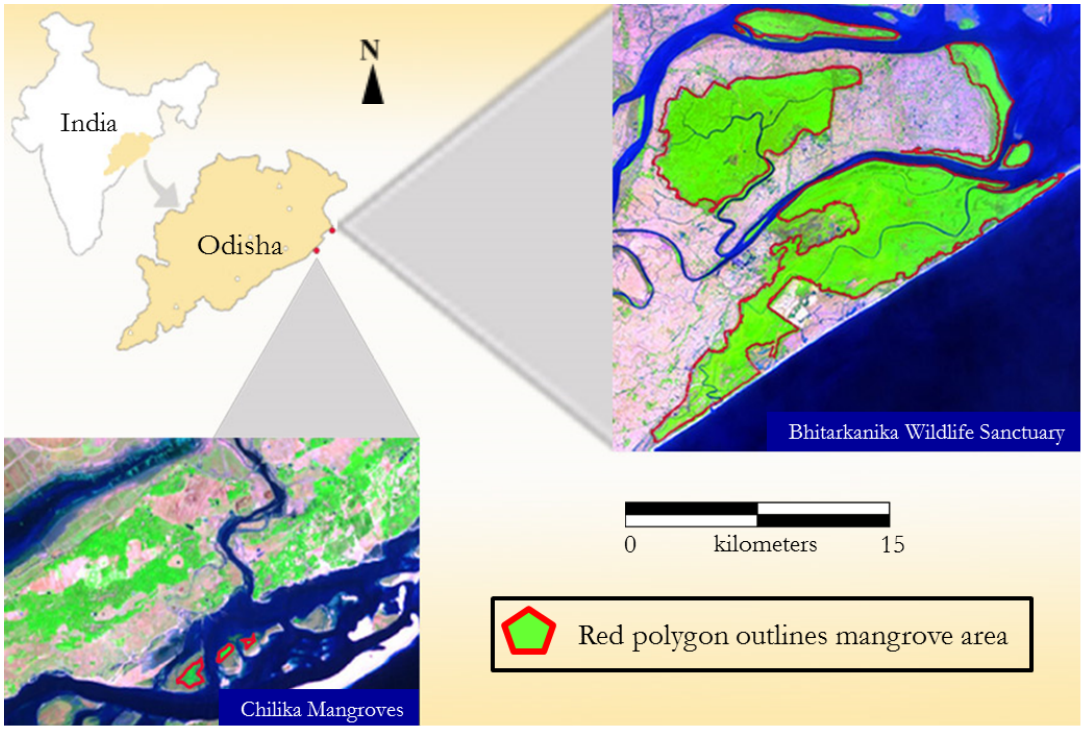

Figure 1. Study area map showing Bhitarkanika Wildlife Sanctuary and Chilika Lagoon. Mangrove patches are outlined by red polygons.

3. Methodology

3.1 Data Acquisition

Satellite data from multiple sensors were downloaded from January 2013 to September 2016 (Table 1). Cloud-free Landsat 8-Operational Land Imager (OLI) surface reflectance (R_{rs}) products were downloaded from the United States Geological Survey (USGS) EarthExplorer website for both Bhitarkanika and Chilika. Terra- Moderate Resolution Imaging Spectroradiometer (MODIS) 250 m Level-2G R_{rs} daily products (MOD09GQ) corresponding to the nearby dates of Landsat 8-OLI data acquisition were downloaded from NASA's Level 1 and Atmosphere Archive and Distribution System (LAADS) website. Terra-Advanced Spaceborne Thermal Emission and Reflection Radiometer (ASTER) Level-1 standard products were also downloaded from USGS EarthExplorer. Sentinel-2 MultiSpectral Instrument (MSI) products were downloaded from the ESA Scientific Data Hub website. In addition to single-day products, 8-day composite products from Terra-MODIS sensor were downloaded from the LAADS website. These 8-day composite products included Level-3 500 m R_{rs} data (MOD09A1), Level-4 Leaf Area Index (LAI) 1 km product (MOD15A2), and Level-4 Net Photosynthesis 1 km product (MOD17A2).

Table 1: Data Acquisition Chart. Cloud-free and nearly cloud-free images were collected from January 2013 to September 2016.

Satellite	**Sensor**	**Product**	**Temporal Resolution**	**Spatial Resolution (m)**	**Source**
Landsat 8	Observational Land Imager (OLI)	Surface Reflectance	16-day	30	USGS EarthExplorer
Terra	Moderate Resolution Imaging Spectroradiometer (MODIS)	Level-2G Surface Reflectance (MOD09GQ)	1-day	250	NASA's Level 1 and Atmosphere Archive and Distribution System (LAADS)
		Level-3 Surface Reflectance (MOD09A1)	8-day	500	
		Level-4 Leaf Area Index (MOD15A2)	8-day	1000	
		Level-4 Net Photosynthesis (MOD17A2)	8-day	1000	
	Advanced Spaceborne Thermal Emission and Reflection Radiometer (ASTER)	Level-1 Standard Product	16-day	15	USGS EarthExplorer
Sentinel-2	MultiSpectral Instrument (MSI)	Top of Atmosphere Reflectance Product	12-day	10	ESA Scientific Data Hub

3.2 Data Processing

MOD09GQ products and standard OLI products were used directly for data extraction as these products were already atmospherically corrected. However, OLI bands (visible and near-infrared (NIR) bands) were stacked using ENVI and then imported to Sentinel Application Platform (SNAP) software for further processing. MOD09GQ products did not require stacking and only contained two bands (red and NIR), so

they were directly imported to SNAP for processing. Conversely, ASTER and MSI images required atmospheric correction prior to any processing. ASTER images were atmospherically corrected using ENVI's atmospheric correction tool, Fast Line-of-sight Atmospheric Analysis of Hypercubes (FLAASH). MSI images were atmospherically corrected using the Sen2cor extension tool in the SNAP software. When all of the atmospherically corrected products were available, these images were processed by using the band math tool in SNAP to extract the R_{rs} from the available bands and the various vegetation indices (Appendix A).

In order to derive the biophysical parameters such as LAI, Gross Primary Production (GPP), and Chlorophyll (CHL), a correlation analysis between R_{rs} (extracted from either individual bands or vegetation indices) and these biophysical parameters was required. However, due to a lack of *in situ* data, these biophysical parameters were not available for the study sites. Therefore, standard MODIS products, such as MOD15A2 and MOD17A2, were downloaded to extract some of these biophysical parameters. Since these are 1km products, MOD09A1 products were downscaled to 1 km using the resampling tool in SNAP. Afterwards, R_{rs} values were extracted from 1 km pixels for correlation with the biophysical data extracted from the MOD15A2 and MOD17A2 products. The best correlation results between vegetation indices and the biophysical parameters were applied to single-date OLI, MODIS, ASTER, and MSI satellite images to create spatio-temporal maps for biophysical variables. Additionally, the single-date OLI images from similar months were averaged based on pixel values to produce monthly composite images, and then processed for biophysical parameters. MODIS images were also averaged monthly using the same procedure and processed subsequently for biophysical parameters.

Although some of the biophysical parameters can be derived using MODIS standard products, MODIS lacked a standard CHL product. Therefore, a CHL model was required to derive the mangrove CHL content from the satellite products. A recent study on mangroves by Pastor-Guzman *et al.* (2015) showed a significant relationship (R^2: 0.78; p=0.0001) between OLI-derived Normalized Difference Vegetation Index (NDVI) and *in situ* mangroves leaf CHL content. From this study, coefficients of the CHL model were directly taken and no re-parameterization was carried out because of lack of field data (Eq. 1). The primary reason for selecting this model was based on the similarities between the climate and seasonality of Pastor-Guzman *et al.* (2015)'s study area (Northwestern Yucatan Peninsula) and our study areas in Eastern India. Pastor-Guzman *et al.* (2015) tested various vegetation indices derived from OLI and correlated to leaf CHL content. More details on the correlation can be found in Pastor-Guzman *et al.* (2015).The following relationship between NDVI and CHL was used to create spatio-temporal maps from satellite images:

$$CHL = (127 * NDVI) - 46.61 \quad (1)$$

3.3 Data Analysis

Data extracted from multiple satellite sensors were analyzed both qualitatively and quantitatively. The qualitative analysis was carried out by observing the time series of biophysical parameter spatial maps and true color satellite images. This time series analysis was based on four different seasons that we recognized around India's monsoon season: Fall (post-monsoon), Winter, Spring, and Summer (dry). The monsoon season was considered as a separate season and included months that had limited satellite data due to heavy cloud coverage. Table 2 lists which months are grouped within each season. True color images were compared with satellite derived biophysical parameters spatio-temporal maps for qualitative comparison.

Table 2. Recognized seasons for Bhitarkanika and Chilika study areas and corresponding months.

Season	**Months**
Fall (post-monsoon)	October and November

Winter	December and January
Spring	February and March
Summer (dry)	April and May
Monsoon	June, July, August, and September

In order to analyze the data from satellite products quantitatively, mean value and standard deviation of CHL, LAI, and GPP was extracted from each satellite image using the statistical tool in SNAP. These data were analyzed based on a monthly and seasonal basis and the results from the MODIS and OLI sensors were plotted using Microsoft Excel. The range of values for all the parameters were carefully observed for the MODIS and OLI sensors and compared against each other using bar graphs.

3.4 Biophysical Model Calibration and Validation

A total of eight (n=8) cloud-free MOD09A1 products corresponding to the Fall, Winter, Spring, and Summer seasons were used to extract the R_{rs} values (Appendix C). Data from the different seasons were incorporated to avoid any seasonal bias in the biophysical model. MOD09A1 products were available at 500m spatial resolution and were downscaled to 1-km resolution to match with the same 8-day time period standard MODIS biophysical products, including LAI (MOD15A2) and GPP (MOD17A2). R_{rs}, LAI, and GPP data were extracted from 20 random pixels (Appendix B) over the Bhitarkanika study area in all 24 MODIS products (8 for each R_{rs}, LAI, and GPP). Six MOD09A1 products that corresponded to all four seasons were used to extract R_{rs} data from 119 pixels (n=119) for model calibration (20 pixels from each product, but 1 pixel was excluded due to cloud coverage). The other two MOD09A1 products were used to represent the Fall (post-monsoon) and Summer (dry) seasons, and from them, 40 R_{rs} data pixels (n=40) were extracted for independent validation. Before model calibration, a spectral analysis was conducted to observe the sensitivity of individual MODIS bands to seasonality. Once the spectral analysis was completed, a correlation analysis was carried out between the individual MODIS bands R_{rs} data (119 pixels) and the biophysical parameters (LAI and GPP). Apart from individual band correlation, various vegetation indices (NDVI, Enhanced Vegetation Index 1 (EVI1), Enhanced Vegetation Index 2 (EVI2), NDVI (Green), Simple Ratio (SR), and Normalized Difference Moisture Index (NDMI)) were also incorporated in the correlation analysis. Coefficients for EVI1 and EVI2 were directly taken from the Pastor-Guzman *et al.* (2015) study. The accuracy of the calibrated model was evaluated in terms of root mean square error (RMSE) and percentage normalized root mean square error (%NRMSE) during independent validation. The models with the least RMSE and %NRMSE were selected to create spatial biophysical map products in order to show seasonal variability in LAI and GPP. CHL spatial maps were created using the Pastor-Guzman *et al.* (2015) OLI based NDVI model (Eq. 1).

3.5 Cross-Calibration of Sensors

MOD09GQ products and standard OLI products did not show significant variability in R_{rs} magnitude most likely because they are both atmospherically corrected with the same procedure. However, other sensors incorporated in this study for enhancing spatial resolution, such as ASTER and MSI products, were not atmospherically corrected. After implementing atmospheric correction procedures on ASTER and MSI images, the resulting products showed differences in their R_{rs} magnitude range. Therefore, to produce consistent biophysical products, cross-calibration between the sensors was required to match the magnitude range of MODIS and OLI. ASTER and MSI are high spatial resolution sensors; therefore, the OLI sensor was chosen to cross-calibrate with these sensors' spectral bands since it had a higher spatial resolution (30 m) than MODIS (250 m). However, it was difficult to obtain co-incident date images for these sensors, which led to the incorporation of nearby date images for cross-calibration. The MSI and OLI time gap was 2 days (MSI: February 01, 2016; OLI: January 29, 2016) and the ASTER and OLI time gap was 7 days (ASTER: March 16,

2016; OLI: March 08, 2016). Since individual bands are more affected by atmospheric scattering, we used vegetation indices (NDVI and EVI2) for cross-calibration and assumed that these indices did not significantly vary between time gaps in image acquisition dates. These two indices (NDVI and EVI2) were used to create spatial biophysical map products. After calibrating these indices against OLI, we were able to match the magnitude range for all the parameters including CHL, LAI, and GPP.

3.6 Seasonal Analysis

Cloud-free OLI products from each month of the years 2013-2016 were collected and combined to calculate monthly averaged composites (excluding months from the monsoon season when cloud-free data was unavailable). Similarly, MODIS images corresponding to nearby dates of OLI were downloaded and averaged for each month. Dates of both MODIS and OLI images used to create averaged composites are provided in the Appendix section (Appendix D). The biophysical models (CHL, LAI, and GPP) were applied to these time averaged products to create spatio-temporal maps for seasonal analysis. The spatial maps produced from the OLI and MODIS sensors were compared against each other to observe variability in pattern and magnitude. Comparison between the sensor results was only carried out for the Bhitakanika study area because the mangrove patches in Chilika were too small to resolve using MODIS low spatial resolution data. However, the seasonal patterns in Chilika mangroves were studied using OLI sensors and compared against the seasonal patterns observed in Bhitarkanika mangroves. Limited availability of MSI and ASTER data restricted us to only using MODIS and OLI for seasonal analysis. All of the above methodology steps are presented in Fig. 2.

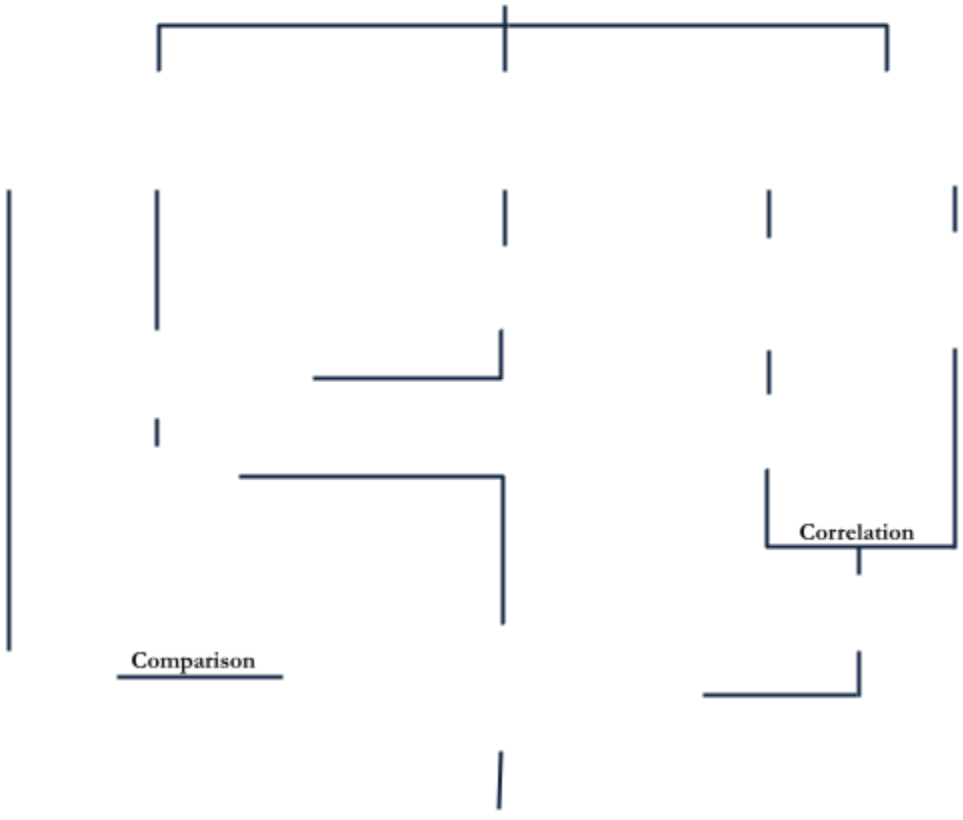

Figure 2: Summary of project methodology

3.7 NASA Giovanni Data

We assumed that the mangroves' biophysical parameters would show seasonal variability, along with potential fluctuations in soil moisture and water salinity. Soil moisture and water salinity values were not available for the study area, but they are known to be closely related to the precipitation patterns (high soil moisture and low water salinity during the monsoon and Fall seasons and opposite during the Summer/dry season). Therefore, we incorporated the Tropical Rainfall Measuring Mission (TRMM) precipitation product from the NASA Giovanni web-based application tool. Monthly precipitation products (TRMM_3B43_v7) from TRMM were first visualized using the NASA Giovanni tool, then corresponding NetCDF files were downloaded for each month between January 2013 and December 2015. These files were further processed in SNAP to extract precipitation data for the entire watershed. Seasonal spatial patterns in precipitation were also presented with transects generated using the NASA Giovanni tool.

4. Results & Discussion

4.1 Seasonal Spectral Variability

The sensitivity of MODIS spectral bands (B1 – B6) during different seasons was clearly distinguished in the spectral signatures extracted from 20 random locations (1 km- pixels) in the Bhitarkanika mangroves (Fig. 3). The visible bands (B3, B4, and B1) showed greater saturation in R_{rs} during the Fall season compared to the NIR and Shortwave Infrared (SWIR) bands (Fig. 3a). This could be because of the post-monsoon saturated land surface, which typically absorbs most of the visible light. In turn, this absorption lowered the R_{rs} magnitude and showed the R_{rs} 20 pixel values at a similar spectral range (coinciding at one point) (Fig. 3a). However, as the land surface became drier during the Winter, Spring, and Summer seasons, the R_{rs} magnitude began to increase in visible bands and reduce in the NIR band (Figs. 3b, 3c, and 3d, respectively). An important observation from this spectral analysis was that during the Fall the R_{rs} magnitude in NIR was relatively higher (mean value: 0.31) and the slope of the red edge (slope between B1 and B2) was steeper (mean value: 0.82), which indicates healthy vegetation. In contrast, during the summer season, the slope of the red edge was significantly reduced (mean value: 0.57), which meant degraded vegetation health. Moreover, the SWIR bands (B5 and B6) had a lower R_{rs} magnitude compared to the NIR band's R_{rs} during the Fall, but then began to gradually increase in magnitude during the following seasons. SWIR1 (B5) even crossed the NIR band in terms of the R_{rs} magnitude during the Summer (Figs. 3a, 3b, 3c, and 3d). The mean spectra for each season was calculated and presented in Fig. 3e. The seasonal variability in R_{rs} in respect to different spectral bands was further utilized for developing the biophysical models.

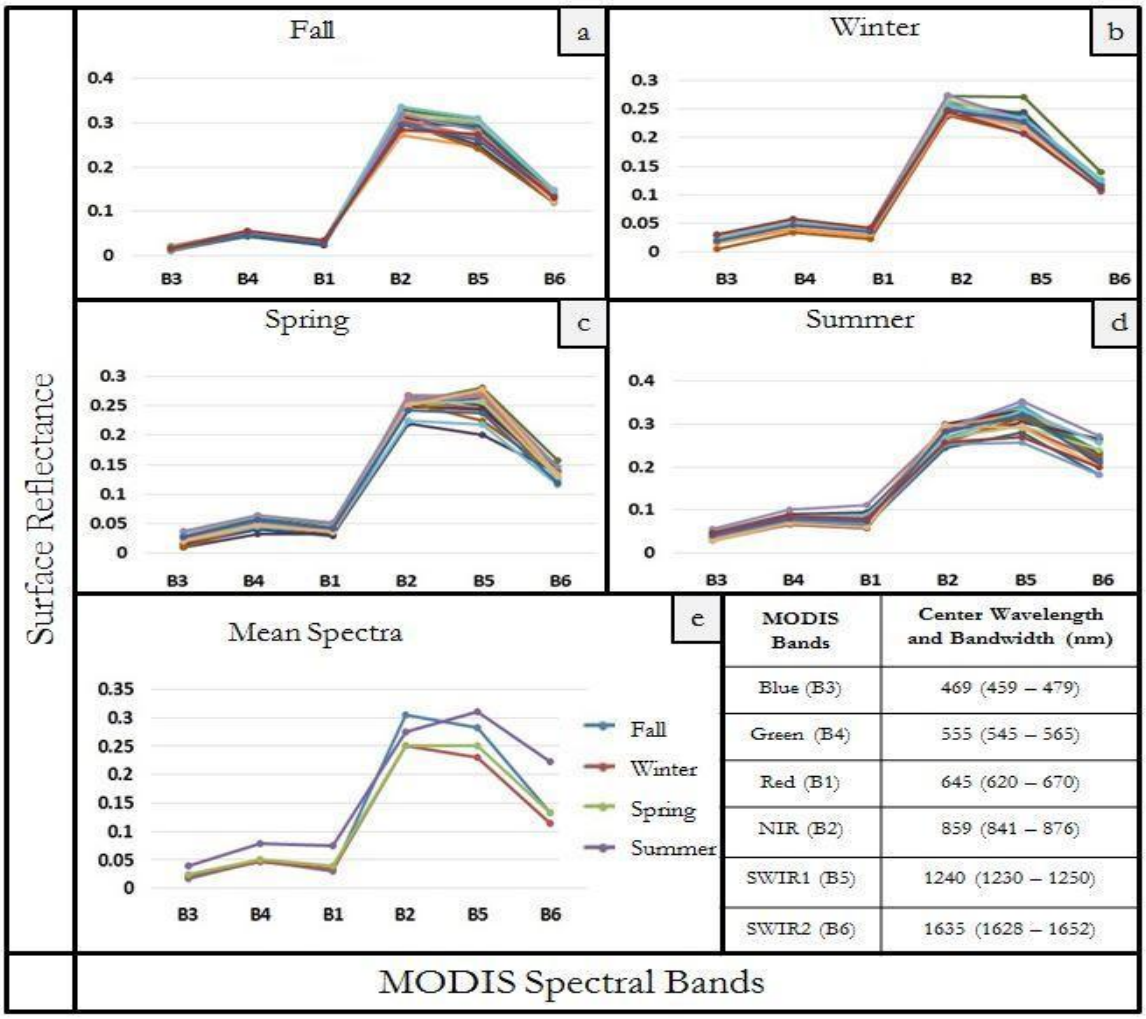

MODIS Bands	Center Wavelength and Bandwidth (nm)
Blue (B3)	469 (459 – 479)
Green (B4)	555 (545 – 565)
Red (B1)	645 (620 – 670)
NIR (B2)	859 (841 – 876)
SWIR1 (B5)	1240 (1230 – 1250)
SWIR2 (B6)	1635 (1628 – 1652)

Figure 3: Seasonal spectral variability corresponding to the MODIS spectral bands. The MODIS surface reflectance spectra was derived from 20 random points from the Bhitarkanika study area after resampling pixels from 500m to 1km to match with the biophysical parameter products (GPP, LAI) which were generated at 1 km resolution.

4.2 Biophysical Model Calibration and Validation

The correlation analysis between the R_{rs} derived from individual MODIS bands and the LAI derived from standard MODIS products revealed that the red band showed the highest correlation ($R=0.69$; $p<0.001$; $n=119$) among other individual MODIS bands for the LAI model calibration (Appendix E). However, when comparing all of the vegetation indices and the individual bands, both EVI1 and EVI2 showed the highest and most significant correlation ($R=0.78$; $p<0.001$; $n=119$) for LAI model calibration (Appendix E). The wide range of data (range: 5.2) was included in the LAI model calibration as shown in Fig. 4a, which was required for a robust biophysical model. An independent validation of LAI models (all individual bands and vegetation indices in correlation to LAI) revealed that EVI2 is the best performing model (RMSE=0.76; %NRMSE=19.54%) compared to all of the individual MODIS bands and vegetation indices based on RMSE and %NRMSE values (Appendix F; Fig. 4b). Therefore, the EVI2-based LAI model was used in this study to create the spatial LAI map products. A similar process was used for calibrating and validating GPP model. Again both EVI performed best among all individual MODIS bands and vegetation indices during GPP

model calibration (R: 0.77; p<0.001; n=119) (Appendix E; Fig. 4c). Furthermore, GPP validation result revealed that EVI2 is the best performing model after comparing its RMSE and %NRMSE (RMSE=0.0053 g-C/m2; %NRMSE=18.64%) with the error values of other indices and individual bands (Appendix F; Fig. 4d). Therefore, EVI2 index was used for creating spatial GPP map products throughout this study.

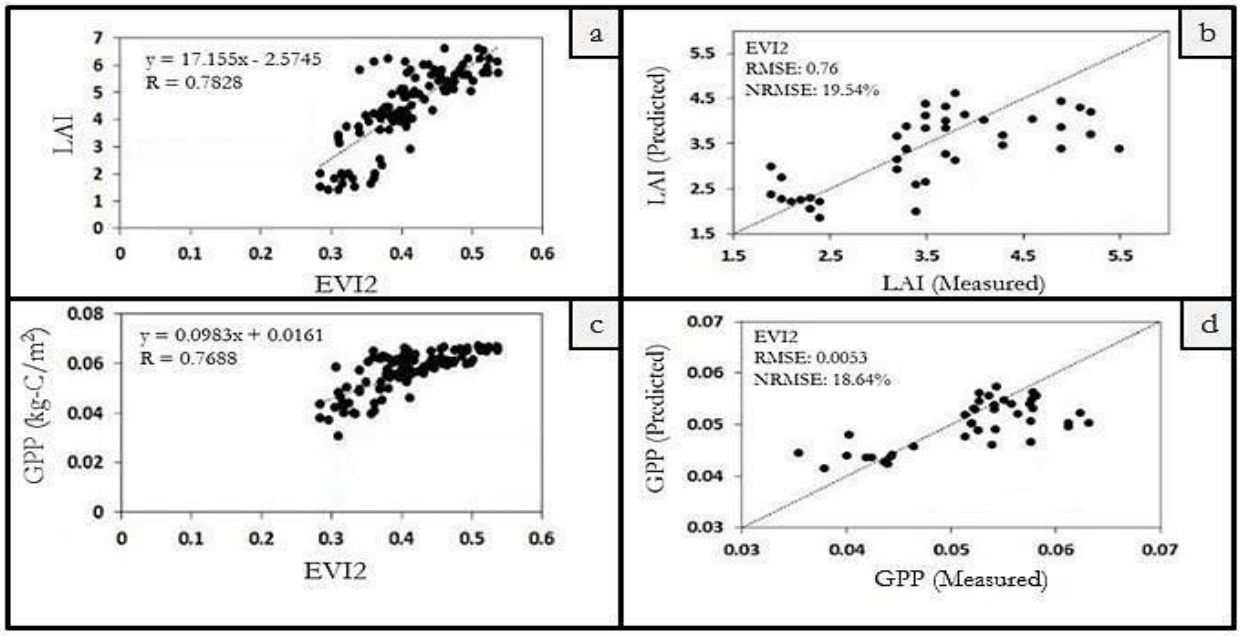

Figure 4: Calibration results for biophysical parameters LAI (a) and GPP (c). A total of 119 R_{rs} data pixels (n=119) from all four seasons were incorporated in the biophysical model calibration. Validation and error estimate results for biophysical parameters LAI (b) and GPP (d). Validation results were derived from an independent data set (n=40) corresponding to different seasons to avoid any seasonal bias.

4.3 Spatio-temporal Analysis

4.3.1 Qualitative Analysis

All the biophysical parameters (CHL, LAI, and GPP) spatial maps created using MODIS and OLI showed similar seasonal pattern corresponding to Bhitarkanika (Fig. 5). Only these two sensors were selected for monthly comparison because of limited availability of data from the ASTER and MSI sensors. Qualitative observation of spatial maps indicated higher values of the biophysical parameters during the Fall, moderate values during the Winter and Spring, and lower values during the Summer. This could be caused by the seasonal variability in soil moisture and water salinity levels within the study area. The Fall season follows the monsoon season (high precipitation); therefore, the land surface area remained wet and the salinity levels are assumed to have stayed low during this season. In contrast, during the Summer, when the land surface area remained dry and the water salinity levels remained high, all of the biophysical parameters were observed at their lowest values (Fig. 5). Several studies have found a negative correlation between high water salinity and leaf biophysical parameters (Bhar *et al.*, 2013; Mitra and Banerjee, 2010; Parida *et al.*, 2003). For example, Parida *et al.* (2003) concluded in their study that high salinity levels reduce photosynthesis in leaves by reducing the diffusion of CO_2 to the chloroplast through stomatal closure and changes in mesophyll structure. This leads to a decrease in the conductance to CO_2 within the leaf and affects the photochemistry of the leaves.

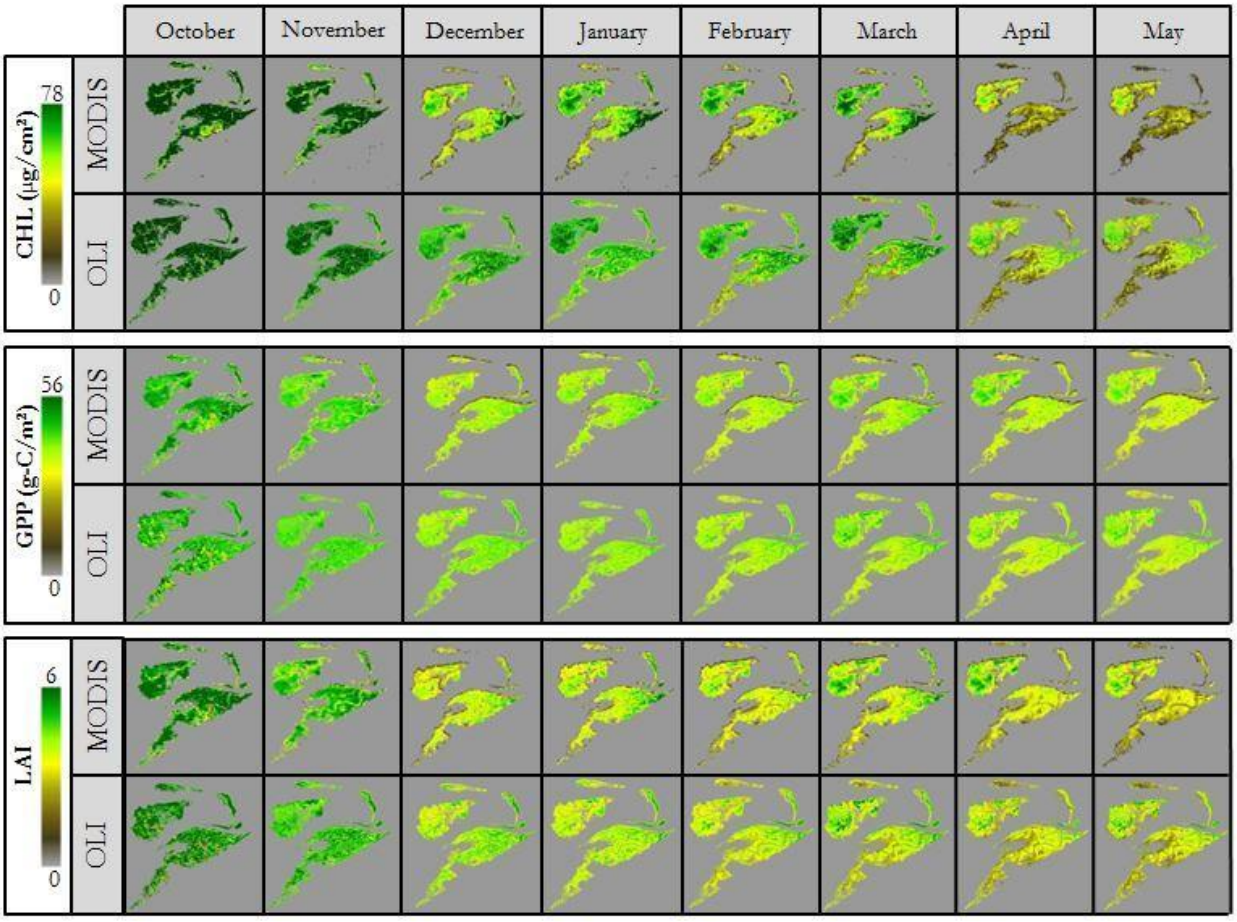

Figure 5: Monthly spatio-temporal variability in mangroves' CHL, GPP, and LAI values (2013-2016) using MODIS and OLI monthly averaged composites. Months within the monsoon season were excluded due to a lack of cloud-free data.

A comparison of Bhitarkanika's and Chilika's seasonal patterns revealed that both study areas followed similar seasonal patterns in their biophysical parameters (Fig. 6). In addition, the true color images clearly distinguished soil conditions during the different seasons. During the Fall, the land surface appeared greener and darker compared to the other seasons because of the saturated land surface post-monsoon. In the following seasons, the land surface gradually became drier and brighter and the mangroves leaf color also displayed variability, which was shown on the biophysical parameters maps (Fig. 6).

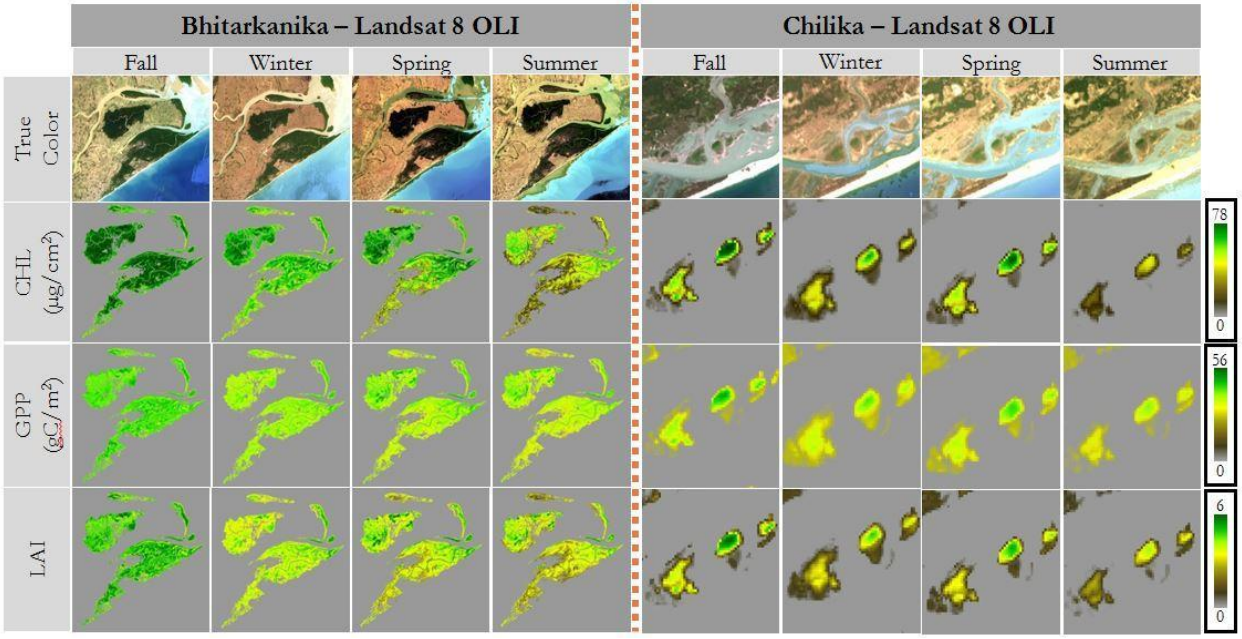

Figure 6: Seasonal changes of each biophysical parameter (CHL, GPP, LAI) for the Bhitarkanika and Chilika mangroves using OLI monthly averaged composites. Fall is represented by a November composite, Winter is a January composite, Spring is a March composite, and Summer is a May composite.

4.3.2 Quantitative Analysis

The MODIS and OLI biophysical parameters showed variation between each sensor's monthly averaged results (e.g. MODIS's December CHL mean: 35.29 ± 14.7 µg/cm^2 versus OLI's December CHL mean: 46.60 ± 5.5 µg/cm^2) (Fig. 7). This could be attributed to the temporal issues faced when creating the monthly averaged composites. The monthly averaged composites for MODIS and OLI neither used same-date images nor did they include the same number of images for each month (Appendix D). Therefore, final composites were possibly affected by the lack of consistent temporal data. Another reason for the variability could be the differences in sensor specifications such as bandwidth and signal to noise ratio (SNR) of the spectral bands used to extract the concentration of biophysical parameters. For example, MODIS has a wide bandwidth for both red (620-670: 50 nm) and NIR (841-876: 35 nm) bands compared to OLI's red (636-673: 37 nm) and NIR (851-879: 28 nm) bands. In addition, the SNR corresponding to MODIS red and NIR bands are 128 and 201, respectively; yet, the OLI red and NIR bands have SNR of 204 and 265, respectively. Despite these issues between the sensors, the most significant finding from the monthly composites was the verification of the seasonal biophysical changes in the mangroves. When comparing the seasonal biophysical parameter results from MODIS and OLI, it can be seen that all three parameters followed a similar pattern. CHL, GPP, and LAI reached peak values in the Fall, moderate values in the Winter and Spring, and low values in the Summer (Table 3). This quantitative analysis supports the results of our qualitative analysis, and helps validate the seasonal biophysical changes in the mangroves.

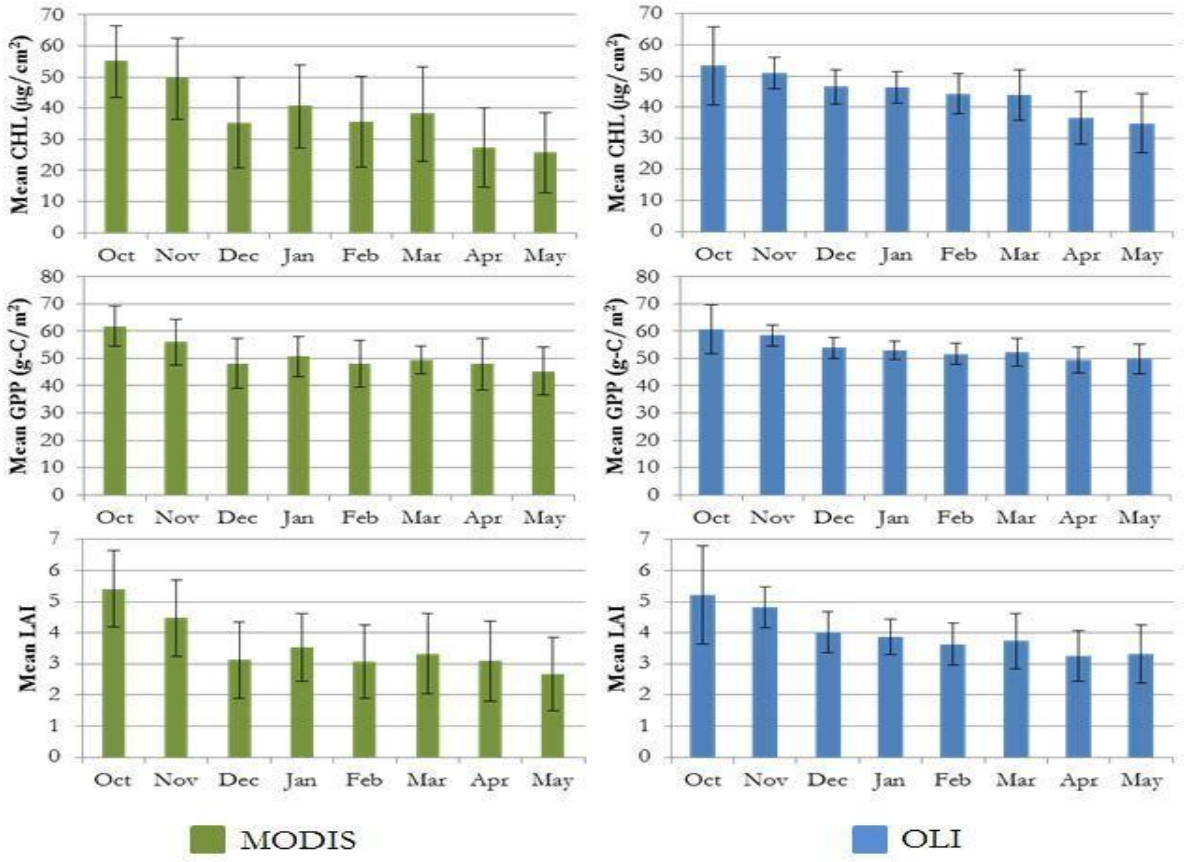

Figure 7. Montly mean values of CHL, GPP, and LAI from MODIS and OLI for the Bhitarkanika mangroves. Standard deviations are represented by the error bars for each month. Months within the monsoon season were excluded due to a lack of cloud-free data.

Table 3. Seasonal mean values of CHL, GPP, and LAI from MODIS and OLI for the Bhitarkanika mangroves. Standard deviation in all the biophysical parameters are included within the paranthesis.

	Fall		Winter		Spring		Summer	
Biophysical Parameters	**OLI**	**MODIS**	**OLI**	**MODIS**	**OLI**	**MODIS**	**OLI**	**MODIS**
CHL ($\mu g/cm^2$)	52.10 (±8.8)	52.23 (±12.4)	46.52 (±5.3)	37.92 (±14.0)	44.14 (±7.3)	36.77 (±14.8)	35.63 (±8.9)	26.46 (±12.7)
GPP ($g\text{-}C/m^2$)	59.60 (±6.5)	58.95 (±7.9)	53.50 (±3.6)	49.45 (±8.2)	51.95 (±4.5)	48.65 (±6.9)	49.65 (±5.1)	46.65 (±9.1)
LAI	5.02 (±1.1)	4.94 (±1.2)	3.95 (± 0.6)	3.32 (±1.2)	3.68 (±0.8)	3.20 (±1.2)	3.28 (±0.9)	2.88 (±1.2)

4.4 Precipitation Analysis

The precipitation values obtained using NASA Giovanni data indicated that the greatest quantity of precipitation in Bhitarkanika falls between June and August (Fig. 8). This is in agreement with the heavy monsoon rainfall for this climatic zone. The spatial pattern of precipitation for one complete year (July 2015-June 2016) was downloaded from NASA Giovanni and shown in Fig. 8a. The satellite data registered the effects of Hurricane Phailin (category 5) in Eastern India in 2013 (Fig. 8b), which caused an unusually high amount of rain during October of that year. Understanding the precipitation patterns in the study area is relevant to understanding changes in mangroves' biophysical characteristics because this factor could impact

net primary productivity, growth and salinity in the mangroves. High soil salinities, a function of the local hydrology and geomorphology, appear to be the most important variable that influences the productivity of mangroves in a given region (Mitsch and Gosselink, 2015). For instance, in a sub-tropical mangrove forest where fresh water availability is seasonal, precipitation patterns could affect the physiological development of the mangrove trees, resulting in an increase or decrease of ground salinity (Lacerda, 2002). The concentrations of leaf pigments, such as CHL, can be associated with environmental factors such as ambient temperature, sunlight, water availability and salinity (Flores-de-Santiago *et al,* .2012). Furthermore, understanding the precipitation patterns at the study area contributes a better accuracy in the estimation of CHL. The accuracy of and selection of vegetation indices estimating leaf CHL can vary according to the season in which the data are collected. Previous studies in mangroves have shown that the CHL concentration of different mangrove species in poor condition showed seasonal dependence, unlike those that were healthy (Flores-de-Santiago *et al.*, 2013).

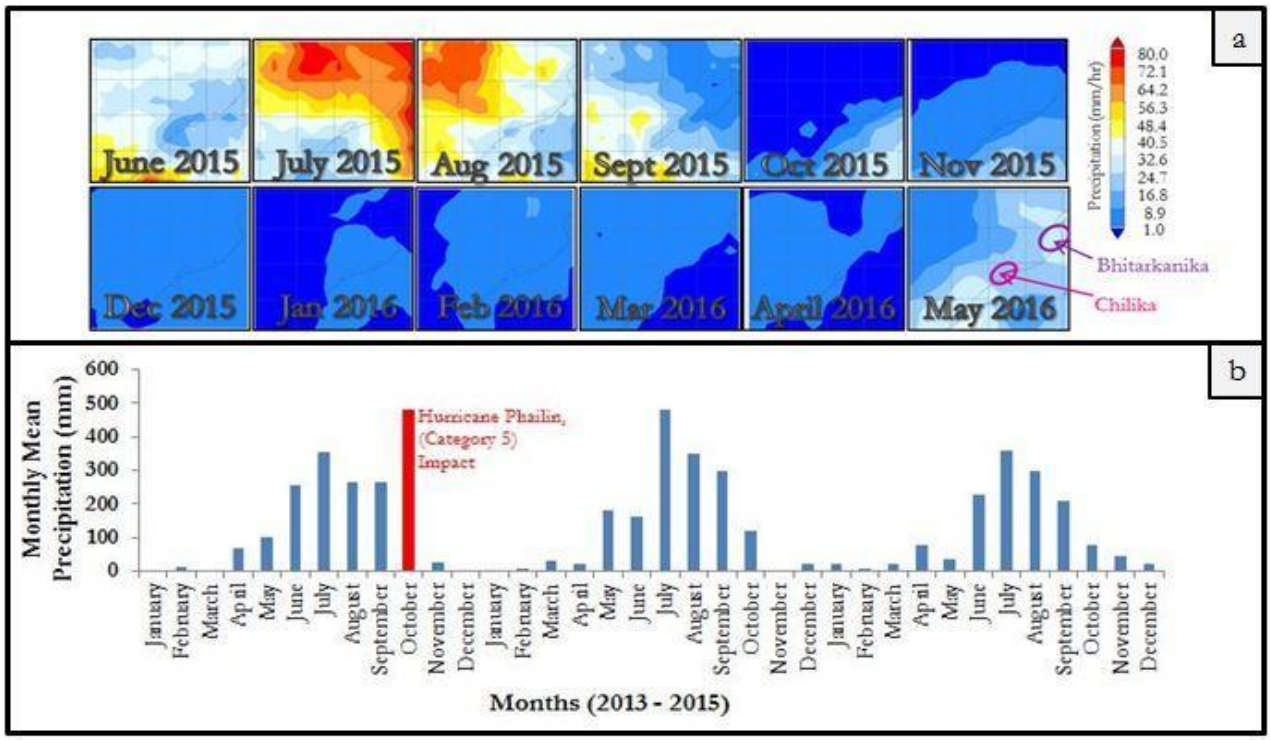

Figure 8. The spatial pattern of precipitation for one complete year (July 2015- June 2016) (a). Monthly mean precipitation (2013-2015) corresponding to the Bhitarkanika watershed, with Hurricane Phailin (category 5) highlighted in red (b). Data from the year 2016 was not included in quantitative analysis because the year is incomplete. All precipitation data was extracted from NASA Giovanni.

4.5 Integrating Satellite Sensors: A Future Perspective

Each sensor has its advantages, so we decided to integrate the sensors to improve both the temporal and spatial monitoring of mangroves health. For example, MODIS has the highest temporal resolution among all the sensors incorporated in this study, and MSI has the highest spatial resolution. Therefore, if data from one sensor was unavailable, but available from the other sensor, then we were able to fill the gaps in the data. However, achieving a similar range of magnitude of biophysical parameters proved to be challenging without cross-calibrating the sensors. Thus, we cross-calibrated the sensors (OLI, ASTER, and MSI) before applying the biophysical models (Appendix G). The results that corresponded to chlorophyll content for a similar

season (Spring) were compared between multiple sensors after implementing the cross-calibration relationship (Fig. 9). However, it was difficult to find data acquired from similar dates and within the same year, especially for MSI and ASTER sensors. This meant that we were not able to compare the results for other seasons during this term of the project; instead the comparison will be conducted next term. Furthermore, it should be noted that MODIS was not cross-calibrated with the other sensors in this study due to its coarse spatial resolution.

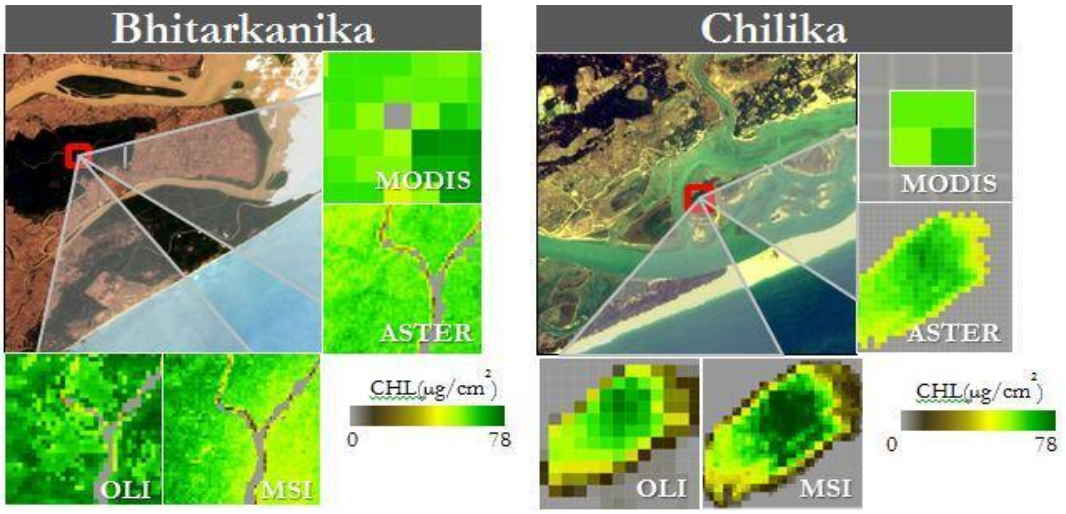

Figure 9: Comparison of spatial resolution between the four sensors. All images were acquired from the Spring season. After cross-calibration of sensors, a similar range of CHL was shown across products. Dates of images are as follows: Bhitarkanika—MODIS – February 9, 2014, ASTER – February 15, 2002*, MSI – February 1, 2016, and OLI – February 8, 2014; Chilika – MODIS – February 15, 2016, ASTER – March 16, 2016, MSI – February 15, 2016, and OLI – February 2, 2016. (*Cloud-free Bhitarkanika ASTER data for the Spring season were unavailable between the years 2013-2016)

5. Conclusions

The methodology used during this study was able to reveal the seasonality of the mangroves' biophysical parameters, such as CHL, GPP, and LAI, which provides a basis for the development of the mangroves biophysical prediction tool. The biophysical parameters followed a similar seasonal pattern reaching peak values in the Fall season, moderate values in the Winter and Spring seasons, and low values in the Summer season. In addition, the comparative analysis between Landsat 8-OLI's and Terra-MODIS's average monthly biophysical parameters showed similar seasonal patterns despite their differences in spatial resolution. This finding implies that other high spatial resolution sensors, including Sentinel-2 MSI and Terra-ASTER, may be used in future studies of the Bhitarkanika and Chilika study areas. In order to utilize these high spatial resolution sensors, cross-calibration would be required, since the atmospheric correction techniques of MSI and ASTER products differ from the techniques applied to OLI's and MODIS's standard surface reflectance products. Data from high spatial resolution sensors proved to be limited within our study period, so including more data that corresponds to the co-incident dates of multiple sensors might improve the cross-calibration results and validate the relationships observed. Moreover, accuracy of biophysical models can be improved in future studies of the Bhitarkanika and Chilika mangroves by incorporating field data.

6. Acknowledgments

We would like to thank our science advisors, Dr. Deepak Mishra and Dr. Marguerite Madden at UGA. We would also like to acknowledge our partners at the Government of Odisha's CDA, especially Dr. Gurdeep

Rastogi for his involvement with the project and international communication during the term. Additionally, our team would like to thank UGA Assistant Center Lead Sean Cameron for his support.

Any opinions, findings, and conclusions or recommendations expressed in this material are those of the author(s) and do not necessarily reflect the views of the National Aeronautics and Space Administration.

This material is based upon work supported by NASA through contract NNL11AA00B and cooperative agreement NNX14AB60A.

7. References

Azam, N. N. A. (2011) The Importance of Mangrove Forests Management. *International Islamic University Malaysia*.

Behera, D. P. & Nayak, L. (2013) Floral Diversity of Bhitarkanika, East Coast of India and its potential uses. *Journal of Chemical, Biological and Physical Sciences, 3*, 1863-1874.

Bhar, S., Chakraborty, D., Ram, S. S., Das, D., Chakraborty, A., Sudarshan, M., and Santra, S. C. (2013) Spatial variation of chlorophyll integrity in a mangrove plant (*Excoecaria agallocha*) of Indian Sundarban, with special reference to leaf element and water salinity. *Journal of Environmental Sicence, Toxicology, andFood Technology, 3(5)*, 24-31.

Chauhan, R. & Ramanathan, A. L. (2008) Evaluation of water quality of Bhitarkanika mangrove system, Orissa, east coast India. *Indian Journal of MarineSciences, 37*, 153-158.

Department of Forest and Environment, Government of Odisha. (2008) State of Environment: Biodiversity Hotspot – Bhitarkanika.

Flores-de-Santiago, F., Kovacs, J., & Flores-Verdugo, F. (2012) Seasonal changes in leaf chlorophyll a content and morphology in a sub-tropical mangrove forest of the Mexican Pacific. *Marine Ecology Progress Series, 444,* 57–68. doi: 10.3354/meps09474

Flores-de-Santiago, F., Kovacs, J. M., & Flores-Verdugo, F. (2013) The influence of seasonality in estimating mangrove leaf chlorophyll-a content from hyperspectral data. *Wetlands Ecology and Management, 21(3),* 193–207. doi: 10.1007/s11273-013-9290-x

Giri, C., Ochieng, E., Tieszen, L. L., Zhu, Z., Singh, A., Loveland, T., Masek, J., Duke, N. (2010) Status and distribution of mangrove forests of the world using earth observation satellite data.*Global Ecology and Biogeography, 20*, 154-159. doi: 10.1111/j.1466-8238.2010.00584.x

Hussain, S. A. & Badola, R. (2010) Valuing mangrove benefits: contribution of mangrove forests to local livelihoods in Bhitarkanika Conservation Area, East Coast of India. *Wetlands Ecology and Management, 18,* 321-331. doi: 10.1007/s11273-009-9173-3

Kauffman, J. B. & Donato, D. C. (2012) Protocols for the measurement, monitoring and reporting of structure, biomass and carbon stocks in mangrove forests. *Center for International Forestry Research*.

Lacerda, L. D. (Ed.). (2002) *Mangrove Ecosystems*. Berlin, Heidelberg: Springer Berlin Heidelberg. Retrieved from http://link.springer.com/10.1007/978-3-662-04713-2

Mitra, A. and Banerjee, K. (2010) Pigments of *Heritiera fomes* seedlings under different salinity conditions: perspective sea level rise. *Mesopotamian Journal of Marine Science, 25(1)*, 1-10.

Mitsch, W. J., & Gosselink, J. G. (2015). *Wetlands (Fifth edition)*. Hoboken, NJ: John Wiley and Sons, Inc.

Parida, A., Das, A. B., and Das, P. (2002) NaCl Stress Cause Changes in Photosynthetic Pigments, Proteins, and Other Metabolic Components in the Leaves of a True Mangrove, *Bruguiera parviflora*, in Hydroponic Cultures. *Journal of Plant Biology 45(1)*, 28-36.

Pastor-Guzman, J., Atkinson, P. M., Dash, J. Rioja-Nieto, R. (2015) Spatiotemporal Variation in Mangrove Chlorophyll Concentration Using Landsat 8. *Remote Sensing* , 7, 14530-14558; doi:10.3390/rs71114530

Pattanaik, C., Reddy, C. S., Murthy, M. S. R., & Swain, D. (2008) Assessment and Monitoring the Coastal Wetland Ecology Using RS and GIS with Reference to Bhitarkanika Mangroves of Orissa, India. *Monitoring and Modelling Lakes and Coastal Environments*, 226-236. doi: 10.1007/978-1-4020-6646-7_17

Peetabas, N. & Panda, R. P. (2015) Conservation and Management of Bioresources of Chilika Lake, Odisha, India. *International Journal of Scientific and ResearchPublications, 5*.

Reddy, S. C & Murthy, M. (2007) Assessment and Monitoring of Mangroves of Bhitarkanika Wildlife Sanctuary, Orissa, India using Remote Sensing & GIS. *Current Science*, *92*, 1409-1415.

8. Content Innovation

Content Innovation #1: VPS

2016Fall_UGA_EasternIndiaEco_VPS_FD_V2.mp4

Content Innovation #2: Glossary

- Advanced Spaceborne Thermal Emission and Reflection Radiometer (ASTER) – an imaging instrument onboard Terra. ASTER data is used to create detailed maps of land surface temperature, reflectance, and elevation.
- Biophysical Parameters – a numerical or other measurable factor derived from in-situ data that can be used to assess changes in wildlife habitat, watersheds, permafrost and vegetation in support of cumulative impact monitoring and ecosystem assessment. Examples include leaf area index, leaf chlorophyll, gross primary productivity.
- Chlorophyll – a green pigment that absorbs sunlight and uses its energy to synthesise carbohydrates from CO_2 and water.
- Gross Primary Productivity – the rate at which ecosystem's producers store and capture provided amount of energy as biomass in a given time duration.
  Landsat 8 – launched on February 11, 2013, the Landsat 8 satellite images the entire Earth every 16 days in an 8-day offset from Landsat 7 and acquires moderate resolution, multispectral images of the globe.

- Leaf Area Index – the total one-sided area of leaf tissue per unit ground surface area.It is defined as the one-sided green leaf area per unit ground surface area (LAI = leaf area / ground area, m^2 / m^2) in broadleaf canopies.
- Mangroves – tropical trees or shrubs that grow in coastal saline or brackish water.
- Moderate Resolution Imaging Spectroradiometer (MODIS) – moderate-resolution imaging spectroradiometer is ideal for tracking large scale changes with its high temporal resolution and 36 discrete spectral bands.
- MultiSpectral Instrument (MSI) – onboard the Sentinel-2 satellite, it collects wide swath (290 km) high-resolution (10 m) images with 13 spectral bands.
- NDVI – an index of plant "greenness" or photosynthetic activity, and is one of the most commonly used vegetation indices.
- Operational Land Imager (OLI) – one of two instruments onboard Landsat 8, the OLI collects image data for nine visible shortwave bands.
- Sentinel-2 – launched on June 23, 2015 by the European Space Agency, the Sentinel-2 satellite's mission is mainly to provide information for agricultural and forestry practices. It expands on the French Spot and US Landsat missions.
- Surface Reflectance (R_{rs}) – ratio of the amount light not absorbed by a surface to the amount of light striking the surface.
- Terra – launched December 18, 1999, the Terra satellite acquires data in 36 groups of wavelengths and promotes understanding of energy balance and climate regimes across the Earth.

Content Innovation #3: Inline Supplementary Materials

- Figure 1. Study area map showing Bhitarkanika Wildlife Sanctuary and Chilika Lagoon.
- Table 1: Data Acquisition Chart.
- Table 2. Recognized seasons for Bhitarkanika and Chilika study areas and corresponding months.
- Figure 2. Summary of project methodology
- Figure 3: Seasonal spectral variability corresponding to the MODIS spectral bands.
- Figure 4: Calibration results for biophysical parameters LAI and GPP.
- Figure 5: Monthly spatio-temporal variability in mangroves' CHL, GPP, and LAI values
- Figure 6: Seasonal changes of each biophysical parameters for the Bhitarkanika and Chilika mangroves using OLI monthly averaged composites.
- Figure 7. Montly mean values of CHL, GPP, and LAI from MODIS and OLI for the Bhitarkanika mangroves.
- Table 3. Seasonal mean values of CHL, GPP, and LAI from MODIS and OLI for the Bhitarkanika mangroves.
- Figure 8. The spatial pattern of precipitation for the year 2015.
- Figure 9: Comparison of spatial resolution between the four sensors.

9. Appendix

Appendix A: All the vegetation indices, their acronym, and corresponding formula used in this study.

Vegetation Indices	**Acronym**	**Formula**
Normalized Difference Vegetation Index	NDVI	$[R_{rs}(NIR)- R_{rs}(B1)]/ [R_{rs}(NIR)+R_{rs}(B1)]$

Enhanced Vegetation Index 1	EVI1	$2.5*[(R_{rs}(NIR)- R_{rs}(B1)])/ (1+R_{rs}(NIR)+6*R_{rs}(B1)-7.5* R_{rs}(B3)]$
Enhanced Vegetation Index 2	EVI2	$2.5*[(R_{rs}(NIR)- R_{rs}(B1)])/ (1+R_{rs}(NIR)+2.4*R_{rs}(B1)]$
Normalized Difference Vegetation Index (Green)	NDVI(G)	$[R_{rs}(NIR)- R_{rs}(B4)]/ [R_{rs}(NIR)+R_{rs}(B4)]$
Simple Ratio	SR	$[R_{rs}(NIR)/R_{rs}(B1)]$
Normalized Difference Moisture Index	NDMI	$[R_{rs}(NIR)- R_{rs}(B6)]/ [R_{rs}(NIR)+R_{rs}(B6)]$

Appendix B: Geographic coordinates of all the 20 random pixel locations used to extract R_{rs} values for spectral analysis and biophysical model calibration and validation.

Points	**Latitude**	**Longitude**
Point 1	20° 42' 45"	86° 50' 36"
Point 2	20° 44' 15"	86° 50' 36"
Point 3	20° 43' 15"	86° 51' 36"
Point 4	20° 42' 15"	86° 51' 06"
Point 5	20° 44' 45"	86° 52' 36"
Point 6	20° 44' 15"	86° 54' 36"
Point 7	20° 42' 45"	86° 51' 06"
Point 8	20° 44' 15"	86° 50' 36"
Point 9	20° 37' 45"	86° 52' 36"
Point 10	20° 41' 45"	86° 56' 36"
Point 11	20° 39' 45"	86° 55' 06"
Point 12	20° 39' 45"	86° 57' 06"
Point 13	20° 41' 45"	86° 58' 06"
Point 14	20° 41' 45"	86° 55' 36"
Point 15	20° 40' 45"	86° 56' 36"
Point 16	20° 39' 15"	86° 54' 36"
Point 17	20° 37' 15"	86° 52' 36"
Point 18	20° 43' 15"	86° 51' 06"
Point 19	20° 41' 45"	86° 51' 06"

Point 20	20° 40' 15"	86° 56' 36"

Appendix C. Time period of MODIS composites (R_{rs}, LAI, GPP products) used for biophysical model calibration and validation. Validation dates are marked with asterisk (*).

MODIS 8-Day Composites	**Starting Julian Date**
1st Week of June, 2015	153
2nd Week of October, 2015	281
3rd Week of October, 2015*	289
2nd Week of November, 2015	313
3rd Week of December, 2015	353
3rd Week of January, 2016	017
4th Week of April, 2016	121
2nd Week of May, 2016*	129

Appendix D. List of all OLI and MODIS images used to create monthly time averaged products for seasonal analysis of biophysical parameters. MODIS images were not included for Chilika due to the inability to resolve the small mangrove patches.

Months	Bhitarkanika		Chilika
	OLI Dates	MODIS Dates	OLI Dates
January	23, 2014 10, 2015 13, 2016 29, 2016	24, 2014 09, 2015 27, 2015	14, 2014 30, 2014 17, 2015
February	08, 2014 24, 2014 27, 2015	09, 2014 25, 2014 26, 2015	02, 2015
March	12, 2014 28, 2014	11, 2014 29, 2014 16, 2015	03, 2014 19, 2014 06, 2015 22, 2015 08, 2016 24, 2016
April	26, 2013 13, 2014 29, 2014	27, 2013 14, 2014 30, 2014	17, 2013 04, 2014 20, 2014

			23, 2015 09, 2016 25, 2016
May	15, 2014	16, 2014 15, 2015	03, 2013 09, 2015 25, 2015
October	25, 2015	23, 2014	29, 2014
November	04, 2013 23, 2014 26, 2015	03, 2013 22, 2014	11, 2013 14, 2014
December	25, 2014	21, 2013 08, 2014 26, 2014	29, 2013 03, 2015

Appendix E. Comparison between different bands and indices correlation results corresponding to LAI and GPP model calibration. These results were derived from 119 pixels R_{rs} data set (n=119) corresponding to all different seasons to avoid any seasonal bias The best result is highlighted in yellow on the table.

Bands & Indices	Abbreviation	Formula	LAI Correlation Coefficient (R)	LAI Correlation Equation	GPP Correlation Coefficient (R)	GPP Correlation Equation
Blue	B3	R_{rs}(B3)	0.64	y= -.93.098x + 6.7841	0.64	y = -0.5418x + 0.0699
Red	B1	R_{rs}(B1)	0.69	y= -55.106x + 6.8859	0.71	y = -0.3287x + 0.0709
Green	B4	R_{rs}(B4)	0.53	y= -54.753x + 7.5682	0.59	y = -0.3543x + 0.0765
Near-InfraRed	B2	R_{rs}(B2)	0.49	y= 24.498x – 2.102	0.45	y = 0.1315x + 0.0212
Shortwave Infrared-1	B5	R_{rs}(B5)	0.1	y= -3.9268x + 5.5421	0.095	y = -0.0218x + 0.0624
Shortwave Infrared-2	B6	R_{rs}(B6)	0.54	y= -18.622x + 7.2501	0.56	y = -0.1126x + 0.0733

Normalized Difference Vegetation Index	NDVI	$[R_{rs}(NIR)- R_{rs}(B1)]/ [R_{rs}(NIR)+R_{rs}(B1)]$	0.69	y= 9.5734x – 2.392	0.73	y = 0.0599x + 0.0135
Enhanced Vegetation Index 1	EVI1	$2.5*[(R_{rs}(NIR)- R_{rs}(B1)])/ (1+R_{rs}(NIR)+6*R_{rs}(B1)-7.5* R_{rs}(B3)]$	0.78	y= 17.009x – 2.6598	0.77	y = 0.098x + 0.0153
Enhanced Vegetation Index 2	EVI2	$2.5*[(R_{rs}(NIR)- R_{rs}(B1)])/ (1+R_{rs}(NIR)+2.4*R_{rs}(B1)]$	0.78	y= 17.155x - 2.5745	0.77	y = 0.0983x + 0.0161
Normalized Difference Vegetation Index (Green)	NDVI(G)	$[R_{rs}(NIR)- R_{rs}(B4)]/ [R_{rs}(NIR)+R_{rs}(B4)]$	0.63	y= 12.398x - 3.6427	0.68	y = 0.078x + 0.0054
Simple Ratio	SR	$[R_{rs}(NIR)/R_{rs}(B1)]$	0.65	y= = 0.3428x + 2.0964	0.67	y = 0.0021x + 0.0421
Normalized Difference Moisture Index	NDMI	$[R_{rs}(NIR)- R_{rs}(B6)]/ [R_{rs}(NIR)+R_{rs}(B6)]$	0.65	y= 7.4622x + 2.3086	0.69	y = 0.046x + 0.0431

Appendix F. Validation result comparison between individual bands and various indices included in the calibration of GPP and LAI. These results were derived from an independent data set (n=40) corresponding to three different seasons to avoid any seasonal bias. The best result is highlighted in yellow on the table.

Bands & Indices	LAI: Root Mean Square Error (RMSE)	LAI: Percentage Normalized Root Mean Square Error (%NRMSE)	GPP: Root Mean Square Error (RMSE)	GPP: Percentage Normalized Root Mean Square Error (%NRMSE)
Blue	1.15	31.89	0.0066	23.63
Red	1.08	30.19	0.0063	22.76
Green	1.33	37.01	0.0076	27.47
Near-InfraRed	0.82	22.88	0.0059	21.26
Shortwave Infrared-1	1.47	40.91	0.0087	31.28
Shortwave Infrared-2	1.42	39.49	0.0082	29.51
Normalized Difference Vegetation Index	1.29	33.32	0.0073	25.64

Enhanced Vegetation Index 1	0.77	19.86	0.0055	19.26
Enhanced Vegetation Index 2	0.76	19.54	0.0053	18.64
Normalized Difference Vegetation Index (Green)	1.28	32.93	0.0072	25.41
Simple Ratio	1.46	37.46	0.011	37.44
Normalized Difference Moisture Index	1.18	30.32	0.0069	24.19

Appendix G. Cross-Calibration of ASTER and MSI with OLI sensor based on indices. Comparison of the mean R_{rs} from the three ASTER bands (green, red, and NIR) with the respective OLI bands revealed significant differences in the green (ASTER: mean R_{rs} = 0.102; OLI: mean R_{rs} = 0.051) and red bands (ASTER: mean R_{rs} = 0.083; OLI: mean R_{rs} = 0.039), but no significant difference in the NIR band (ASTER: mean R_{rs} = 0.245; OLI: mean Rrs = 0.245). This could be because of the different atmospheric correction processes used for these products, along with the higher degree of atmospheric scattering of shorter wavelengths, which can create more variability. Similar to ASTER, mean R_{rs} spectra in the four sentinel bands (blue, green, red, and NIR) showed variability in regards to the OLI respective bands as the atmospheric correction procedure for MSI products is different from OLI's correction process. In addition to visible bands, the NIR band also showed variability in magnitude. Observing this variability in the individual bands, we decided to calibrate the vegetation indices used to create the biophysical products rather than to calibrate the individual bands which are more sensitive to atmospheric correction. We assumed that the indices NDVI and EVI did not changed significantly between the time gaps of image acquisition for the different sensors. Significant correlation between the sensors OLI vs. ASTER and OLI vs. MSI for both indices was observed for ASTER (NDVI: R= 0.81; $p<0.001$; EVI2: R= 0.87; $p<0.001$) and MSI (NDVI: R= 0.88; $p<0.001$; EVI2:

R= 0.87; p<0.001). This calibration result was implemented to ASTER and MSI products to match the magnitude range for biophysical parameters obtained from the OLI sensor.

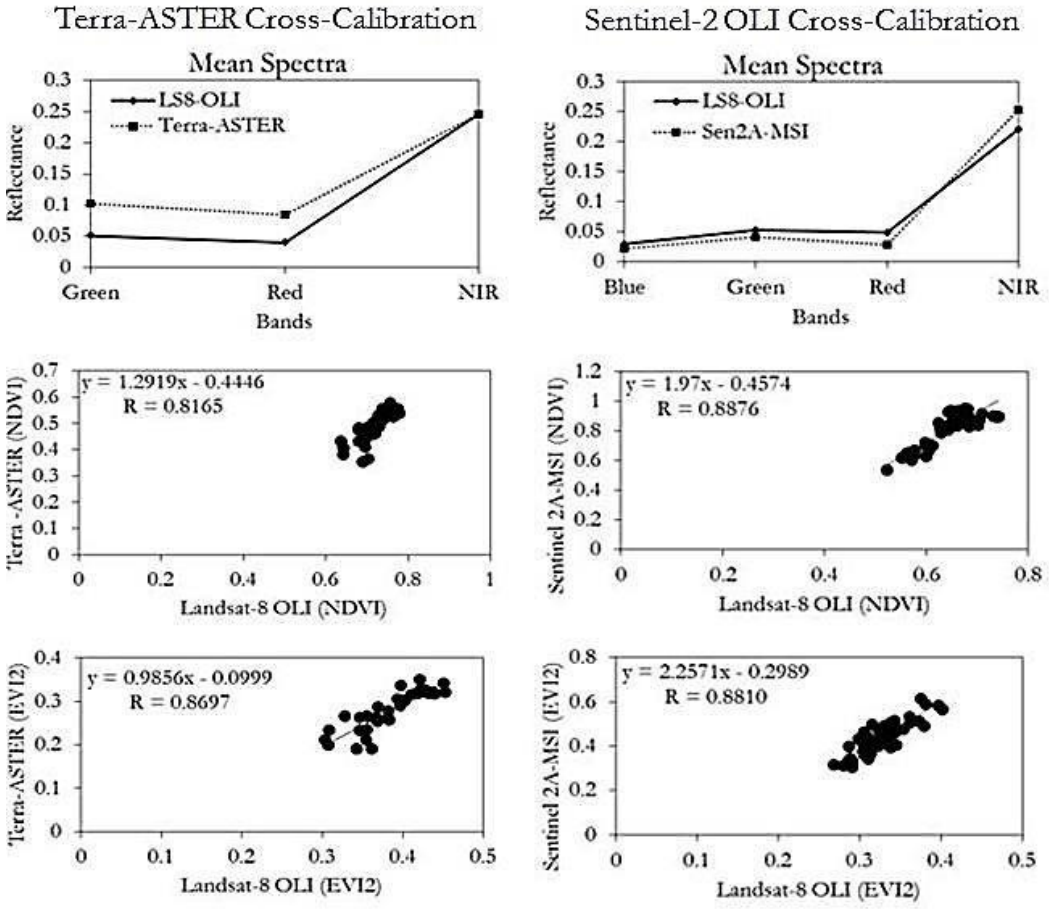

Appendix H. Correlation analysis of MODIS individual bands and various vegetation indices corresponding to LAI model calibration.

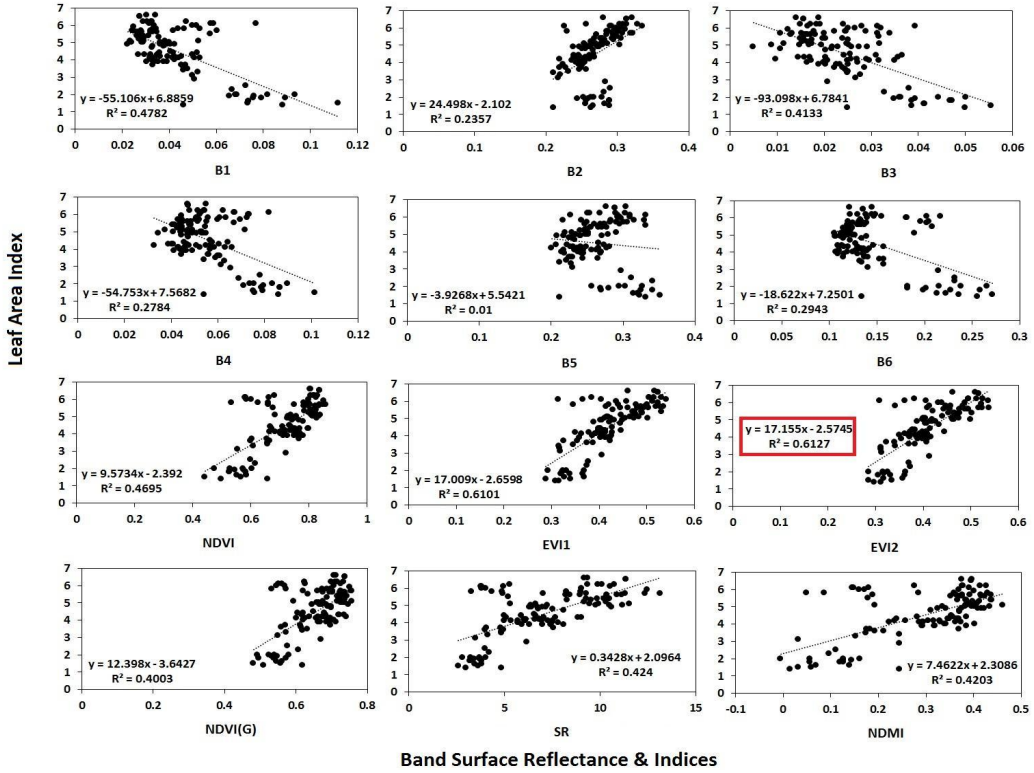

Appendix I. Comparison of validation results for MODIS individual bands and various vegetation indices for LAI model.

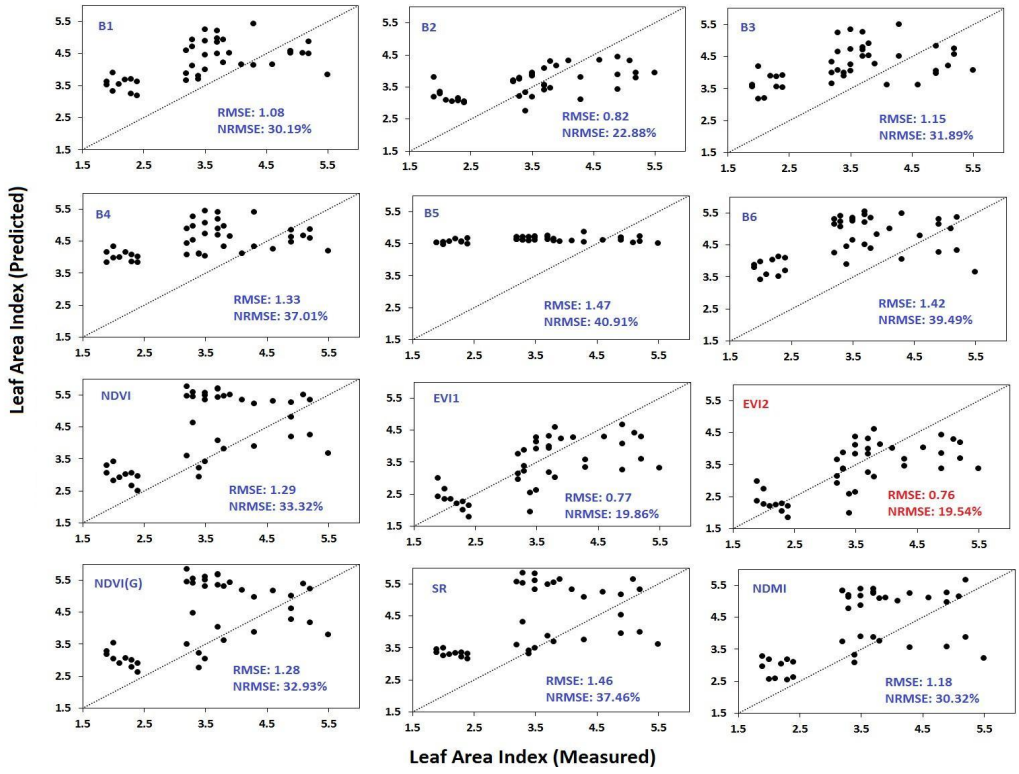

Appendix J. Correlation analysis of MODIS individual bands and various vegetation indices corresponding to GPP model calibration.

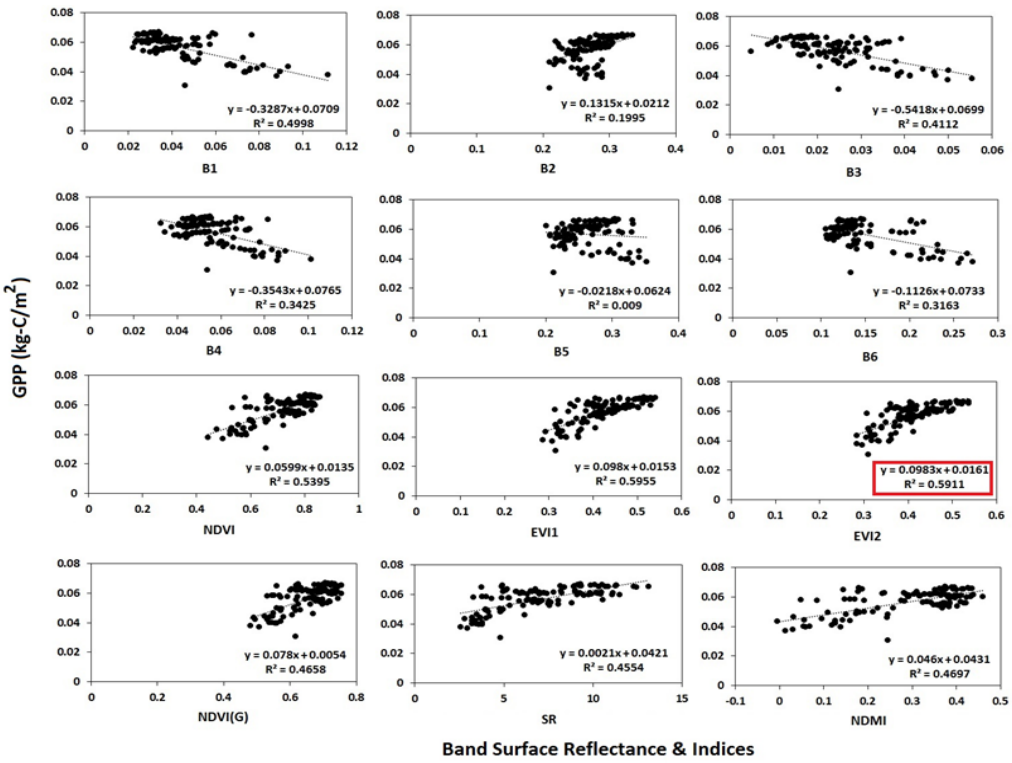

Appendix K. Comparison of validation results for MODIS individual bands and various vegetation indices for GPP model.

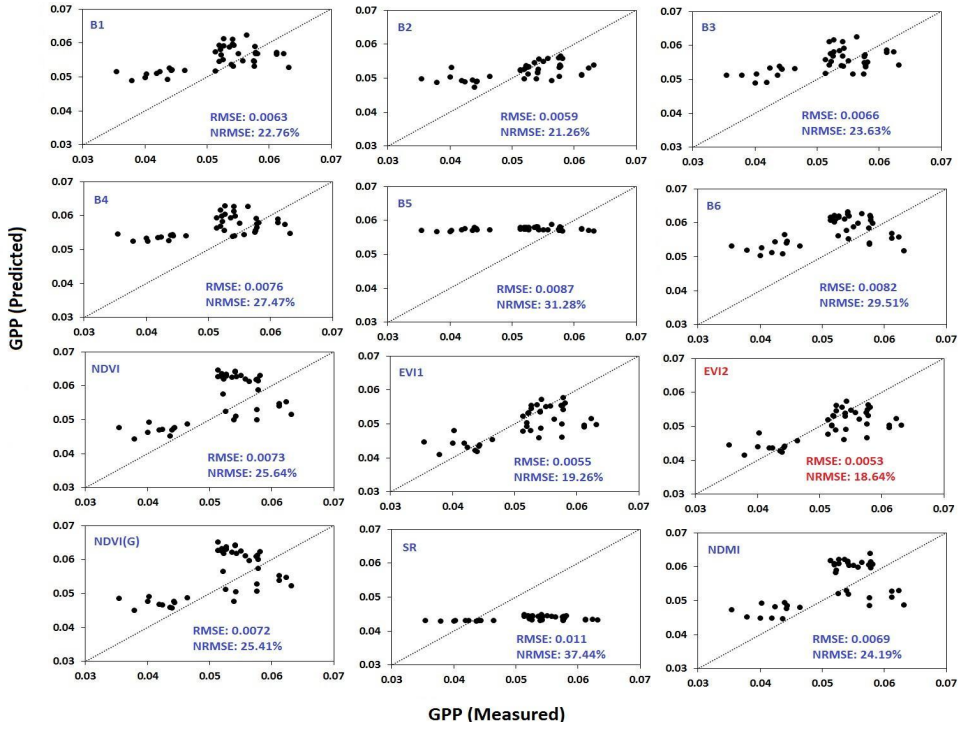

Appendix L. Correlation analysis between biophysical parameters (GPP (a) and LAI (b)) and FPAR. Total of 119 pixels (these are same pixels which were used for calibration of biophysical models) from four seasons (Fall, Winter, Spring, and Summer) were used to establish these relationships.

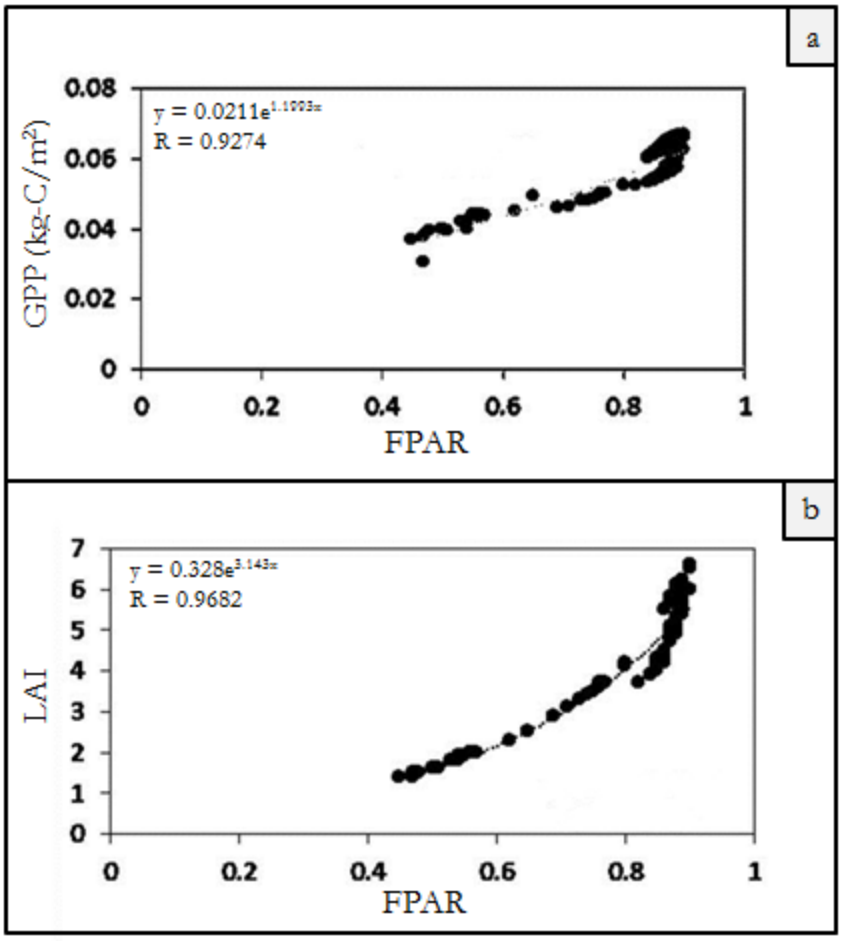

Appendix M. Spatio-temporal pattern of CHL estimates from single-date OLI images (2013-2016). Only cloud-free and distortion-free images were included.

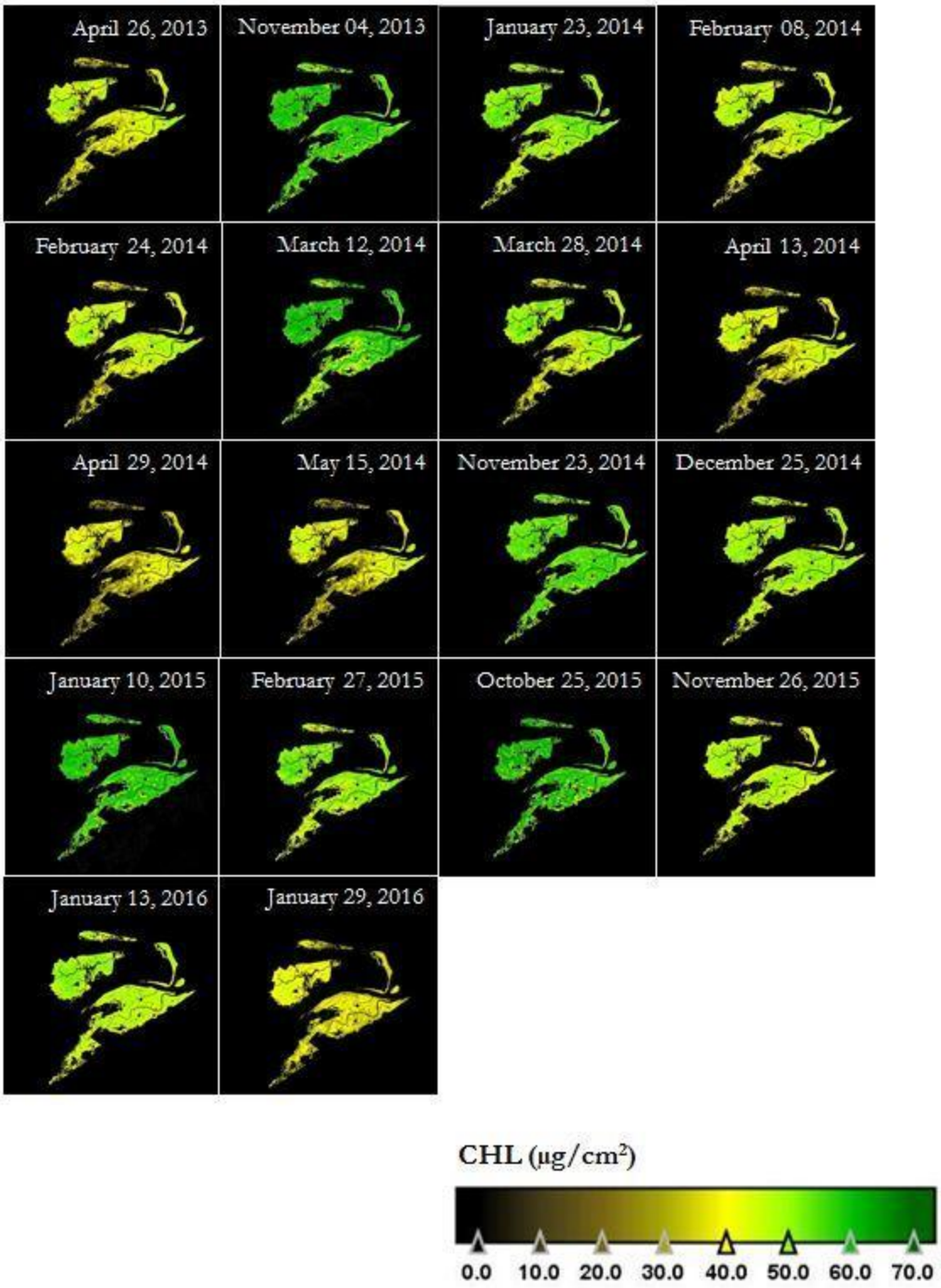

Appendix N. Spatio-temporal pattern of CHL estimates from single-date MODIS images (2013-2015). Only cloud-free and distortion-free images were included.